American Mineralogist, Volume 92, pages 1325–1333, 2007

Structural state of microcrystalline opals: A Raman spectroscopic study

Albena Ilieva,[1] Boriana Mihailova,[2,*] Zdravko Tsintsov,[1] and Ognyan Petrov[1]

[1]Central Laboratory of Mineralogy and Crystallography, Bulgarian Academy of Sciences, Acad. G. Bonchev Street 107, 1113 Sofia, Bulgaria
[2]Mineralogisch-Petrographisches Institut, Universität Hamburg, Grindelallee 48, D-20146 Hamburg, Germany

Abstract

The structure of natural hydrous silica is complex and its study requires the complementary application of several methods. To elucidate the structural state of opaline silica of different geneses, microcrystalline opals from siliceous rocks, geodes, and bentonite clays from East Rhodopes, Bulgaria, were analyzed by Raman spectroscopy, X-ray powder diffraction, electron microscopy, and thermogravimetric and differential thermal analysis. Comparison of X-ray diffraction and spectroscopic data for a series of microcrystalline opals showed that the fraction of tridymite-like structural units can be estimated using the relative intensity of the Raman scattering near 350 cm^{-1}. Opals displaying an intense, poorly resolved Raman band centered near 330–360 cm^{-1} contain a larger proportion of nanosized spatial regions with tridymite-type atomic arrangements as opposed to cristobalite-type arrangements. The results demonstrate the ability of Raman spectroscopy to characterize the fine-scale structure of opal and to better distinguish opals showing similar XRD patterns. The application of Raman micro-spectroscopy showed that on intermediate-range scale the atomic structure of opal lepispheres is closer to the framework topology of tridymite than to that of cristobalite.

Keywords: Opal, Raman spectroscopy, lepispheres, cristobalite, tridymite

Introduction

Hydrous SiO_2 phases are widespread in volcanogenic-sedimentary rocks associated with post-volcanic hydrothermal activity, devitrification, and diagenetic alteration. Opals are micro- and non-crystalline forms of hydrated silica with a high degree of structural disorder, and the structural state of these hydrous silica phases is still not entirely understood. Several authors have shown that precise structural analysis of opals in siliceous rocks can be important for genetic reconstructions. Based on powder X-ray diffraction (XRD) data, Jones and Segnit (1971) distinguished three hydrous silica phases at low temperatures: amorphous opal (opal-A); disordered cristobalite with significant tridymitic stacking (opal-CT); and more ordered cristobalite with minor tridymitic stacking (opal-C). Opal-CT and opal-C are considered as microcrystalline varieties of hydrous silica (Flörke et al. 1991). Opal-C exhibits an XRD pattern strongly resembling that of α-cristobalite. The differences between α-cristobalite and opal-C consist of slight broadening of the Bragg reflections, a slight shift to larger *d*-spacings and a weak extra peak near 4.30 Å for the latter, all of which are due to the presence of tridymite-type layers within the cristobalite structure (Elzea et al. 1994). The main criteria to distinguish opal-CT from opal-C are the position and the width of the most intense Bragg reflection (Flörke et al. 1991; Elzea et al. 1994). For opal-C the *d*-spacing is closer to the position of the strongest reflection of α-cristobalite, whereas for opal-CT it is closer to the position of the second most intense peak of tridymite and may reach 4.13 Å. Opal-CT exhibits broader Bragg reflections and the full width at half maximum (FWHM) of the major peak in 2θ units is >5.6°. In addition, the peak near 4.30 Å and the shoulder near 3.87 Å, which correspond to Bragg reflections of tridymite, are more pronounced for opal-CT.

Flörke et al. (1991) proposed that opal-CT has a unidimensionally disordered three-layered structure of low cristobalite with tridymite-type stacking faults in the [111] direction. Modeling of the XRD patterns has confirmed that the structure of opal-CT consists of an interstratification of cristobalite-like and tridymite-like layers with a variable probability of tridymitic stacking of ~50% (Graetsch et al. 1994; Guthrie et al. 1995). The small crystallite size and the abundance of stacking faults hamper the unambiguous determination of the predominant structural species in opal-CT using only XRD data, and it is particularly difficult to determine fine-scale structural information using XRD.

Using transmission electron microscopy (TEM) and infrared spectroscopy, Wilson et al. (1974) concluded that the dominant phase in the opal-CT samples was essentially α-tridymite with a high degree of stacking disorder. Later, using electron diffraction analysis Akizuki and Shimada (1979, according to Iijima 1988) revealed the absence of cristobalite domains in some opaline silica samples with XRD patterns typical of opal-CT. The authors proposed that this material be designated as opal-T, but its place in the nomenclature of the microcrystalline silicas has not been discussed further. On the other hand, high-resolution TEM on volcanic opaline samples suggested that low cristobalite is the fundamental structural component of opal-CT (Nagase and

* E-mail: mi0a007@uni-hamburg.de

0003-004X/07/0809–1325$05.00/DOI: 10.2138/am.2007.2482

Brought to you by | Florida Atlantic University
Authenticated
Download Date | 11/3/15 9:59 AM

Akizuki 1997). Elzea and Rice (1996) analyzed several opal samples using XRD and high-resolution TEM and demonstrated that the structure of both opal-C and opal-CT consists of a continuous series of intergrowths with cristobalitic and tridymitic end-members. The authors mentioned that tridymite stacking is very common, even prevalent, for opals with a main reflection positioned near 4.1 Å, although they did not introduce the term "opal-T" in their study.

Spectroscopic techniques have also been applied in the study of the opal structure. De Jong et al. (1987) demonstrated that opals with similar XRD patterns can be distinguished using NMR spectroscopy. According to the ^{29}Si NMR data obtained by Adams et al. (1991), the short-range order in opal-CT resembles that of amorphous silica, whereas infrared absorption spectra point to a similarity between opal-CT and tridymite (Rice et al. 1995).

Raman scattering is an ideal method for the study of heterogeneous silicas because of its ability to detect the presence of nano-sized domains of a definite polymorph as well as of non-crystalline substances. Due to the specific physical nature of the inelastic light scattering process, Raman spectroscopy allows one to probe the fine-scale structure of silicates, i.e., to identify the structure-building units composed of a few silicon-oxygen tetrahedra, regardless of the degree of long-range ordering. The Raman spectroscopic method can identify topologically non-equivalent framework silicates via the position of the most intense signal arising from the so-called bridging-oxygen breathing mode of the SiO_4 rings building the structure (Sharma et al. 1981; Dutta et al. 1991; Sykes and Kubicki 1996; Lazzeri and Mauri 2003). In some cases, Raman spectroscopy can distinguish clearly two phases exhibiting similar XRD patterns. A typical example is moganite and quartz (Kingma and Hemley 1994). However, Raman spectroscopy has been applied only sporadically to opals. Smallwood et al. (1997) showed that the Raman spectra of opal-CT from volcanic environments correlated fairly well with the spectrum of α-tridymite. Ostrooumov et al. (1999) demonstrated the sensitivity of Raman spectroscopy to the local structure of opals and its potential to be used for characterization of opals of different geological origin. Rodgers and Hampton (2003) and Fritsch et al. (2004) applied Raman spectroscopy to identify silica phases, including opals, in mineral assemblages.

The objectives of this paper are (1) to analyze the Raman spectra of a series of microcrystalline opals (opal-C and opal-CT) that, according to their XRD patterns, gradually increase in the concentration of tridymitic stacking sequences; and (2) to study the structural state of opaline silica of different geneses from East Rhodopes, Bulgaria, using complementary X-ray diffraction and Raman spectroscopic methods.

Materials and methods

Samples

Nineteen opal samples with different genesis from East Rhodopes, Bulgaria, were investigated in this study. Herein we present the data on selected representative samples (Table 1). Samples S1–S4 were chosen to form a series of opals with different content of tridymitic component as revealed by XRD, whereas the series S5–S8 represents opaline silicates of different geological age. Specimens that appeared by eye optically homogeneous were separated from the main body of the opal samples to be analyzed. Plates of opal polished on one side were prepared for Raman measurements.

Methods

Powder XRD measurements were performed on a DRON 3M diffractometer with a horizontal Bragg-Brentano goniometer (radius of 192 mm) using a Fe-filtered Co$K\alpha$ radiation (40 kV, 28 mA). A step-scan technique was applied with a step size of 0.02 °2θ and 3 s per step in the range 10–50 °2θ. The positions of the reflections were determined by fitting the XRD patterns using the Winfit software package (Krumm 1994).

The morphology of the opal samples was studied by scanning electron microscopy (SEM) using a Philips 515 apparatus and by TEM using a Philips EM 420T with an EDAX 9100 for elemental analysis of the samples. Atomic-emission spectroscopy with inductively coupled plasma (SPECTRO Analytical Inst.) was applied to the samples from geodes to analyze the trace element content. Thermogravimetry (TG) and differential thermal analysis (DTA) were performed on a Stanton Redcroft thermal analyzer STA 780 to 1000 °C with a heating rate of 10 °/min in static air.

Raman spectra were collected with a dispersive and an FT-Raman spectrometer, using an excitation wavelength of 514.5 and 1064 nm, respectively. FT-Raman spectroscopic measurements were performed when the luminescence overlapped the Raman scattering excited by visible light. In that case a Bruker Equinox 55 FT-IR spectrometer equipped with an FRA106/S FT-Raman module was used, applying an output laser power of 0.35 W and a spectral resolution of 4 cm^{-1}. Raman spectra from different spatial regions were recorded with a triple monochromator system Horiba Jobin-Yvon T64000 equipped with an Olympus BH2 microscope. The linear size of the laser spot on the sample surface was about 1.5 μm, while the beam power on the sample surface was kept to 10 mW. The spectral resolution achieved in the micro-spectroscopic measurements was 2 cm^{-1}. The Raman spectra of samples S1–S4 were recorded by both the spectrometers to verify the reproducibility of the experimental data in terms of peak positions and relative intensities. The vanishing of the continuous background when the excitation-light wavelength was changed from 514.5 to 1064 nm clearly indicated that the background of the spectra collected with the 514.5 nm emission line of an Ar^+ laser is due to electronic transitions rather than to additional light scattering processes. In addition, when a microscope was used, Raman spectra were collected from different spatial regions to check the reproducibility of the spectral data. Sporadically, spectra of quartz and chalcedony overlapping the opal spectrum were collected from micrometer-sized areas, which under optical microscope appeared more transparent than the main substance. The spectra of these areas were not further considered. For quantitative analysis of the Raman scattering below 600 cm^{-1} the spectra measured with the Horiba Jobin-Yvon T64000 were used, because of the better elimination of the Rayleigh scattering and the higher effective Raman cross section of the 514.5 nm excitation line used. The spectra were baseline corrected for the continuous luminescence-induced background using an appropriate polynomial function of the LabSpec software package and then fitted with Voigt functions using Origin 6.1. The baseline correction did not affect the peak positions nor their relative intensity ratio. The Raman spectra of opaline samples were compared with the spectra of low cristobalite, monoclinic tridymite, and synthetic vitreous silica (Suprasil), measured with a Horiba Jobin-Yvon T64000 spectrometer

Results and discussion

The chemical compositions of opal samples studied are presented in Table 2. The water contents were determined on the basis of weight loss as detected by TGA. The TG-DTA data displayed a thermal behavior that is typical for hydrous silica. Endothermal effects involving weight losses appear in the temperature range 100–600 °C, but they are not well defined and merge in one broad, poorly structured band. For this reason we calculated the entire weight loss in the range 20–800 °C.

Typical SEM images of different spatial regions in the samples are shown in Figure 1. The micrometer-scale aggregates, or lepispheres, were observed in all of the samples studied (Figs. 1a and 1b). They are built up of randomly oriented bladed crystallites and have been reported by many authors for opals of different genesis, including deep-sea cherts, opoki, agates, etc. (Graetsch 1994). Coloform aggregates composed of differently sized globules, which resemble the "cauliflower" morphology typical of low cristobalite, were observed in sample S6 (Fig.

Brought to you by | Florida Atlantic University
Authenticated
Download Date | 11/3/15 9:59 AM

TABLE 1. Sample characteristics and origin

Sample	Characteristics	Origin
S1	semi-transparent, white-bluish, cracked, fracture flinty	dense-opal geode localized in Paleogene volcanic rocks, products of irregular, multi-stage, hydrothermal activity in East Rhodopes (Rabovo village, Haskovo district)
S2	semi-transparent, whitish, cracked, fracture flinty	dense-opal geode localized in Paleogene volcanic rocks, products of irregular, multi-stage, hydrothermal activity in East Rhodopes (Rabovo village, Haskovo district)
S3	non-transparent, "dirty"-white, dense, fracture unequal	hollow agate geode localized in Paleogene volcanic rocks, products of irregular, multi-stage, hydrothermal activity in East Rhodopes (Rabovo village, Haskovo district); horizontally banded opal specimen from the surface of the geode cavity
S4	non-transparent, white, dense	opal rocks localized in a Paleogene volcanogenic-sedimentary complex (Svetoslav village, Haskovo district)
S5	non-transparent, waxy yellow to yellow-brownish	Neogene sandstones containing opalized wood (Ahmatovo formation, Haskovo district)
S6	non-transparent, white	opal-siliceous rocks in the upper levels of a Paleogene volcanogenic-sedimentary complex (lower Oligocene, Ol_1) forming beds and lenses built up of massive opal alternating with rhyolitic tuffs (Svetoslav village, Haskovo district)
S7	non-transparent, "dirty"-white, cracked	opal-siliceous rocks in the upper levels of a Paleogene volcanogenic-sedimentary complex (lower Oligocene, Ol_1) from a region characterized by high tectonic activity (Perperek village, Kardjali district)
S8	nanosized platy grains clustered onto montmorillonite flakes (TEM data)	fraction < μm containing montmorillonite, opal and calcite from a bentonite clay deposit in the lower levels of Ol_1 of a Palaeogene volcano-sedimentary complex (Entchets village, Kardjali district)

1c). Such morphology was also observed in opal samples from Neogene sandstone crust rocks. Sample S6 exhibits regions with a "tube-like" morphology (Fig. 1d), which has also been observed in zeolitized tuffs from the volcano-sedimentary complex of East Rhodopes.

Figure 2 shows a TEM image typical of the montmorillonite-cristobalite association observed in the clay fraction separated from the bentonite sample S8. The common "cloud-like" morphology of the montmorillonite particles is seen in close association with aggregates of nanoscale cristobalite grains. The chemical composition of the latter indicates that the grains are composed mainly of SiO_2 (about 90 wt%). The remaining elements detected (Fe, Mg, Al) correspond well to the cation content typical of montmorillonite.

The XRD patterns of samples S1–S4 are shown in Figure 3a. From sample S1 to S4 the position of the strongest reflection shifts from 4.05 to 4.10 Å and the peak width increases from 0.3 to 1.0 °2θ Co$K\alpha$ (see Table 3), revealing an increase in the tridymitic component from sample S1 to S4 (Graetsch et al. 1994). In addition, the reflection near 4.30 Å and the shoulder near 3.89 Å are much more pronounced for S3 and S4 as compared to S1 and S2. Therefore, according to the conventional classification, samples S1 and S2 are regarded as opal-C, whereas S3 and S4 are opal-CT.

The Raman spectra of the same samples are presented in Figure 3b. The samples exhibit strong Raman scattering between 200 and 600 cm^{-1}, which is typical of framework silicates, and in the range 3000–3600 cm^{-1}, generated by the O-H bond stretching modes of the hydrous species incorporated in the silicate matrix. The latter band is two-component (signals near 3230 and 3355 cm^{-1}) and is very similar to that generated from the stretching modes of liquid water, which suggests that it is dominated by the contribution of physisorbed water molecules. For comparison, the spectra of low cristobalite, monoclinic tridymite, and silica glass are also included in Figure 3b. The most intense Raman peaks of vitreous silica are at 460 and 490 cm^{-1}, whereas cristobalite is characterized by strong sharp Raman signals at 418 and 231 cm^{-1}. The structure of tridymite is still somewhat of an enigma, and a variety of superstructures has been identified (Smith 1998). The Raman spectra of tridymite samples having similar XRD patterns may differ from each other, but strong Raman scattering between 300 and 405 cm^{-1} is always observed (Etchepare et al. 1978; Gage and Farwell 1981; Hirose et al. 2005; Kihara et al. 2005; Kingma and Hemley 1994). Most probably, the variation in the Raman spectrum of tridymite depends on the predominant type of deformation of the Si-O rings, which mirrors the presence of different tridymitic modifications (Kihara et al. 2005). According to the data published so far, there are three types of Raman scattering of tridymite: (1) the spectrum of monoclinic tridymite, containing four strong Raman signals at 351, 304, 433, and 209 cm^{-1}, the succession follows the peak intensity (Kihara et al. 2005; this paper); (2) a spectrum with a strongest peak near 405 cm^{-1} and several weaker Raman signals in the range 370–152 cm^{-1}; according to single-crystal diffraction analysis the symmetry of this tridymite is triclinic (Etchepare et al. 1978; Kingma and Hemley 1994); and (3) a spectrum with a strongest peak near 365 cm^{-1} and several weaker Raman signals in the range 300–220 cm^{-1}, which was recognized as the spectrum of the higher-temperature orthorhombic modification of tridymite

TABLE 2. Chemical composition of the opal samples studied

Oxide wt%	S1	S2	S3	S4	S5	S6	S7
SiO_2	98.10	97.90	99.45	94.31	87.99	94.80	94.65
Al_2O_3	<0.03	0.19	0.12	0.21	0.60	1.09	1.22
Fe_2O_3	0.10	<0.03	<0.03	0.68	3.68	0.33	0.39
Na_2O	<0.03	<0.03	<0.05	0.11	–	–	–
K_2O	0.04	0.18	<0.05	0.17	–	–	–
MgO	<0.02	<0.02	<0.01	0.12	–	–	–
CaO	<0.02	<0.02	<0.02	0.19	0.11	0.10	0.16
MgO	<0.02	<0.02	<0.01	0.12	–	–	–
ΣH_2O*	1.58	1.96	1.16	2.34	8.24	3.83	3.27
Sum	99.78	100.23	100.73	98.25	100.62	100.15	99.69

* Water content from TGA data.

Brought to you by | Florida Atlantic University
Authenticated
Download Date | 11/3/15 9:59 AM

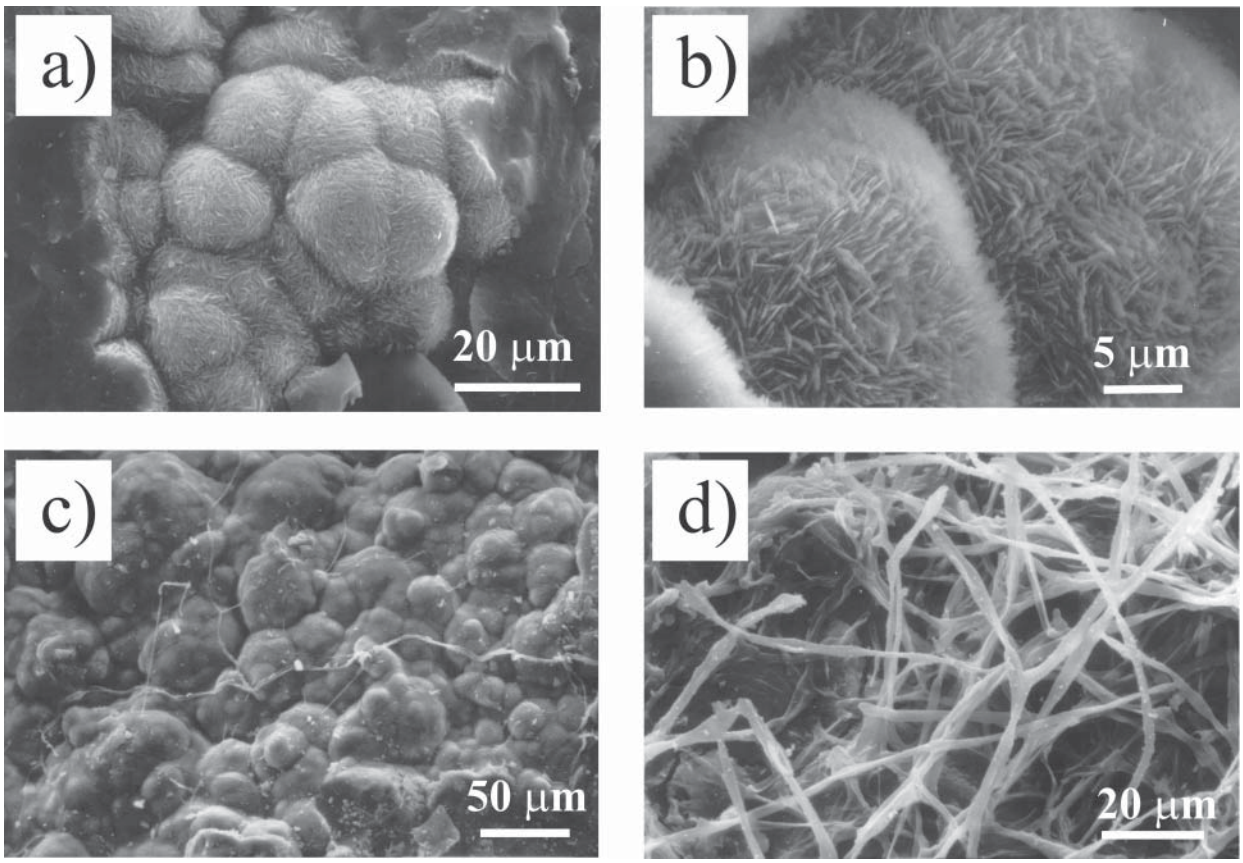

Figure 1. SEM micrographs of opal samples: (**a**, **b**) lepispheres, scale bars 20 and 5 μm, respectively; (**c**) coloform aggregates, scale bar 50 μm; (**d**) "tube-like" morphology, scale bar 20 μm.

(Gage and Farwell 1981; Hirose et al. 2005; Kihara et al. 2005). It is noteworthy that among all natural silica polymorphs only tridymite exhibits the most intense Raman scattering near 350 cm^{-1} (Gage and Farwell 1981; Hirose et al. 2005), whereas low cristobalite does not have a Raman peak at that wavenumber. Therefore, Raman scattering at about 350 cm^{-1} in the opal spectrum is indicative of tridymite-like structural units.

Opal samples S1–S4 possess no resolved signals at 460 and 490 cm^{-1}, which are typical of amorphous silica, suggesting that the fraction of non-crystalline material, if any, is low, below the sensitivity of the experimental technique. It is worth noting that the Raman cross-section of most of the studied opal samples was close to that of vitreous silica. Only sample S1 showed a relatively high cross section, but still lower that that of well-crystalline silica polymorphs as quartz or α-cristobalite. The spectrum of S1 is almost the same as that of cristobalite and the presence of tridymitic species is revealed by additional weak, broadened Raman scattering in the 300–400 cm^{-1} range. The spectrum of S2 contains much more intense Raman scattering at 293 and 361 cm^{-1} and broader "cristobalite" peaks at 414 and 225 cm^{-1}. The former points to an increase in the amount of tridymitic structural units, whereas the latter suggests an increase in the concentration of defects in the cristobalite matrix. The spectral data for S1 and S2 are in a good accordance with the XRD data: (1) for

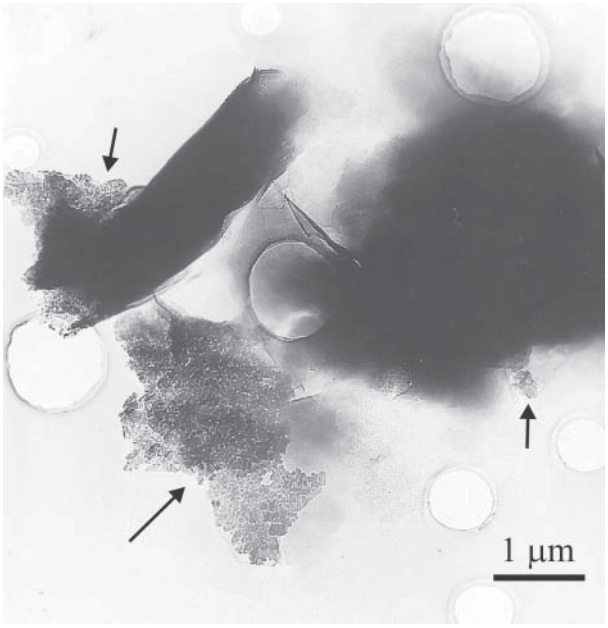

Figure 2. TEM image of montmorillonite-cristobalite association in bentonite samples; arrows point to cristobalite species.

Brought to you by | Florida Atlantic University
Authenticated
Download Date | 11/3/15 9:59 AM

TABLE 3. XRD and Raman data for samples S1–S4

Sample	XRD data*			*R*1†			*R*2			*R*3			*R*4			η	ξ
	d (Å)	FWHM (°)	*L* (nm)	ω	I_{rel}	Γ	ω	I_{rel}	Γ	ω	I_{rel}	Γ	ω	I_{rel}	Γ		
S1	4.05	0.31	21.3	226	0.36	25	285	0.08	64	369	0.06	50	417	0.50	23	0.14	2.2
S2	4.09	0.51	12.2	225	0.25	52	293	0.16	66	361	0.23	67	414	0.36	42	0.39	1.6
S3	4.10	0.76	8.5	226	0.13	71	304	0.35	75	359	0.32	64	412	0.20	60	0.77	1.1
S4	4.10	0.99	6.5	228	0.08	81	302	0.31	73	352	0.37	82	412	0.23	104	0.78	0.8

* *d* and FWHM are the position and full width at half maximum of the most intense Bragg reflection, respectively, determined after fitting the XRD patterns with the Winfit software package; *L* is the corresponding linear crystallite size, calculated from the Scherrer equation applied to the most intense Bragg reflection.
† *R*1 = related mainly to the cristobalite peak at 231 cm^{-1}; *R*2 = related mainly to the tridymite peak at 304 cm^{-1}; *R*3 = related to the tridymite peak at 351 cm^{-1}; *R*4 = related mainly to the cristobalite peak at 418 cm^{-1}; ω (in cm^{-1}), I_{rel}, and Γ (in cm^{-1}) are the peak position, relative intensity, and full width at half maximum, respectively; $\eta = \frac{I(R2)+I(R3)}{I(R1)+I(R2)+I(R3)+I(R4)}$ and $\xi = \Gamma(R3)/\Gamma(R4)$.

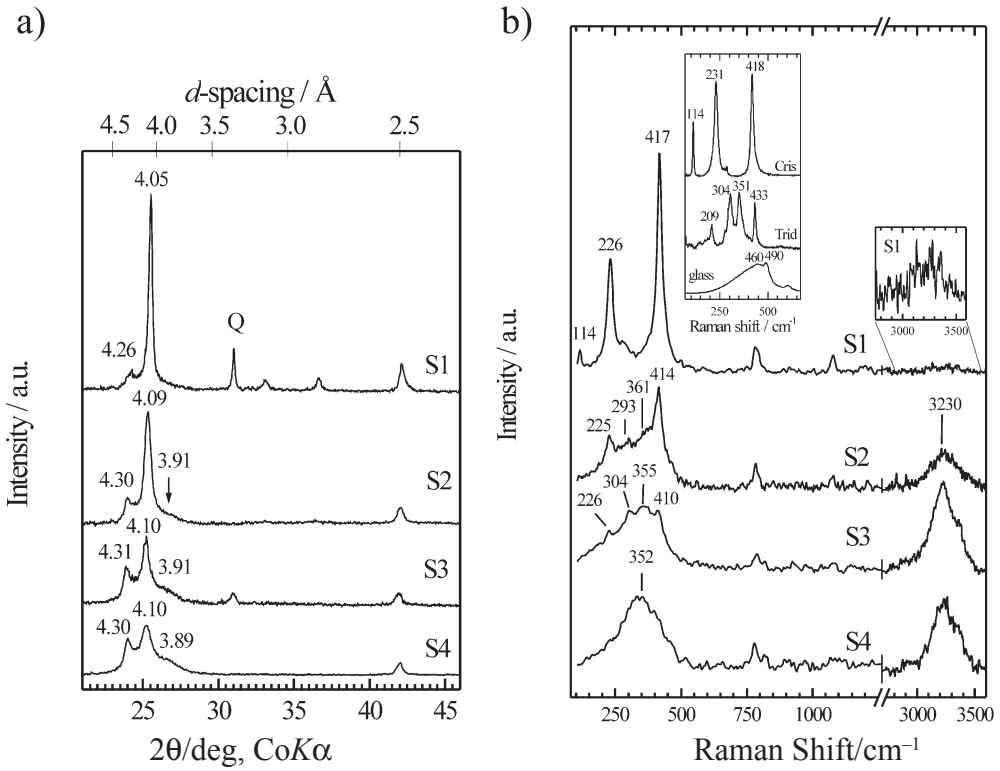

FIGURE 3. (**a**) XRD patterns and (**b**) Raman spectra of samples S1–S4. Q in **a** denotes the most intense Bragg reflections of quartz. In **b** the spectral range 2750–3600 cm^{-1} for S1 is enlarged in Y-axis to display better the water band; the left-hand side inset shows from top to bottom the reference spectra of α-cristobalite, monoclinic tridymite, and silica glass.

both samples cristobalite is the dominant structural component, i.e., they are of the opal-C type, and (2) the degree of stacking disorder is higher for S2 than for S1.

Although the XRD patterns of S3 and S4 are qualitatively the same, the Raman spectrum of S3 differs from that of S4. Four resolved signals were seen in the range 200–600 cm^{-1} for sample S3, but only one broad poorly structured band centered at 352 cm^{-1} was observed for sample S4. Taking into account the gradual changes in the XRD patterns from S1 to S4 (see Table 3) as well as the spectral features of S1 and S2, we assigned the Raman signals at 410 and 226 cm^{-1} in the spectrum of S3 to nanoscale spatial regions with a cristobalite-type atomic arrangement, and the peaks at 355 and 304 cm^{-1} to tridymite-type nanoscale spatial regions. For sample S3 the "cristobalitic" and "tridymitic" Raman peaks are nearly the same in intensity and width, suggesting that the structure of S3 is somehow closer to the "true" opal-CT type: a matrix of intergrown tridymite- and cristobalite-type nano-domains. The dominant Raman scattering near 350 cm^{-1} reveals the abundance of tridymite-type nano-regions for S4. The large broadening and the absence of well resolved Raman signals between 200–600 cm^{-1} point to high degree of disorder also on a scale with a characteristic length of several SiO_4 tetrahedra.

As tridymite transforms into cristobalite via a reconstructive phase transition, it is reasonable to assume that connectivity defects and, consequently, voids for hydrous species occur with a higher probability in the vicinity of the stacking faults, i.e., near the C-T nano-region linkages. The spectra shown in Figure 3b were measured from monolithic opal samples with a penetration length of the excitation light of ~500 μm. As men-

Brought to you by | Florida Atlantic University
Authenticated
Download Date | 11/3/15 9:59 AM

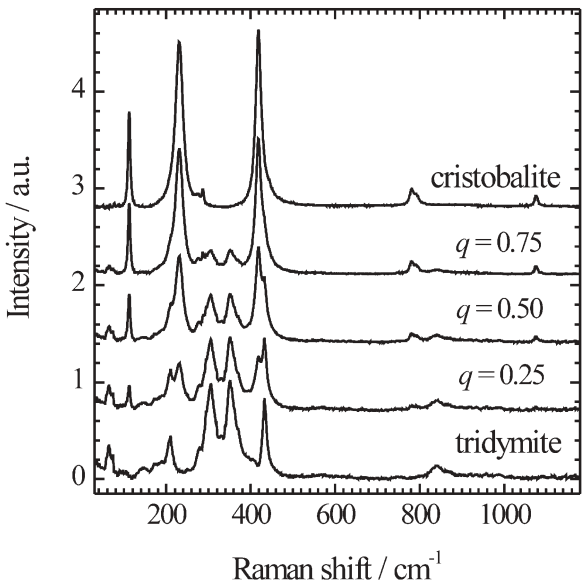

FIGURE 4. Raman spectra of cristobalite and monoclinic tridymite measured under the same experimental conditions together with calculated linear combinations of the cristobalite and tridymite spectra $S = q \times S_{cristobalite} + (1 - q) \times S_{tridymite}$ with different weight coefficients q.

tioned above, the band at 3000–3600 cm^{-1} resembles in shape and position that of liquid water. Hence, the Raman scattering among 3000–3600 cm^{-1} is dominated by the stretching modes of physisorbed, loosely bonded water, which is difficult to determine by DTA/TG analysis because it is released from the bulk sample at the very initial stage of heating. Thus, the relative amount of loosely bonded water occluded in voids in the bulk opal can be estimated from the ratio ρ between the integrated intensity of bands 3000–3600 and 200–600 cm^{-1}, generated from O-H bond stretching and SiO_4-ring modes, respectively. It is reasonable to assume that the content of water is relatively low for microcrystalline opal with low degree of cristoballite-tridymite intergrowth and vice versa. Indeed, the content of physisorbed water is smallest for S1 (ρ = 0.18), which exhibits the lowest degree of stacking disorder and increases for S2 (ρ = 0.78) due to higher stacking disorder compared with S1. The water concentration is highest for S3 (ρ = 1.52) and decreases for S4 (ρ = 1.24), suggesting that the amount of C-T interlayer linkages is higher in S3 than in S4.

One should mention that cristobalite has a higher Raman cross-section than does tridymite and for a hypothetical defect-poor cristobalite-tridymite mixture of ratio 1:1 the Raman scattering arising from the cristobalite crystallites would dominate the spectrum (see Fig. 4). The presence of structural disorder in microcrystalline opal would lead to a broadening of the corresponding Raman peaks. Therefore, on the basis of Raman spectra the portion of cristobalite in opal may be overestimated, but not underestimated.

To better understand the structural state of opals, we performed non-linear curve fitting of the Raman spectra of samples S1–S4 (Fig. 5). The shape of the spectral peaks is also informative in terms of the degree of order. A non-zero Gaussian component in addition to the natural Lorentzian shape reveals statistical disorder in the structural species generating the corresponding Raman peaks. We considered the range 130–600 cm^{-1} and fitted the spectrum profiles of opaline samples with four Voigt functions for the following reasons: (1) In this spectral range the Raman scattering of both opal and reference samples is highly polarized, thus indicating that the peaks arise from the so-called oxygen-breathing ring modes characteristic of a three-dimensional 4-2 connected Si-O network (Barrio et al. 1993). Silicon-oxygen rings are the structural units identifying the structural topology of framework silicates. They represent the intermediate-range ordering of the structure. In terms of ring modes, the observed Raman signals are considered as generated from A_g-modes of the corresponding rings, which explains the high polarization of the peaks. The ring-mode approach is particularly suitable for entirely or partially disordered materials, in which the translational symmetry is violated, as well as for crystalline materials with a large number of atoms in the primitive cell (e.g., zeolite-type framework silicates). It has been found that the wavenumbers of the ring modes correlate with the number of SiO_4 tetrahedra that build the ring and are sensitive to the ring geometry (Sharma et al. 1981; Dutta et al. 1991; Mihailova and Konstantinov 1997). Therefore, the spectral range 130–600 cm^{-1} best represents the fine-scale structure of microcrystalline opals. (2) As discussed above, one should expect at least four Raman signals: near 230 and 415 cm^{-1} related to the cristobalite-like domains and near 300 and 350 cm^{-1} related to the tridymite-like domains; the use of a larger number of peaks led to a strong mutual dependence of the fitting parameters and the fitting procedure failed without imposing extra constraints on the peak positions and widths; and (3) we fitted the Raman spectra using either Lorentzians or Voigt functions (Lorentzian + Gaussian). A Gaussian contribution to the peak profile points to statistical distribution over the possible equilibrium configurations of the structural species that generate the corresponding mode. In the case of opal samples, the use of Lorentzians led to uncertainty in the peak widths and intensities and thus to ambiguous fitting results. For samples S1 and S2 rational fits were obtained when Voigt functions (Lorentzian-to-Gaussian ratio of 1) were used for the Raman scattering at 290 and 360 cm^{-1}. These signals are associated with the tridymite structural fraction and the necessity to introduce a Gaussian component indicates the higher degree of disorder in the tridymitic domains than in the cristobalitic matrix. In contrast, for samples S3 and S4 Voigt functions were successfully used for the Raman signals at 225 and 410 cm^{-1}, suggesting that in these samples the cristobalitic component is more defective than the tridymitic component.

The peak parameters obtained after fitting the spectrum profiles are given in Table 3. Several quantitative trends can be seen for the sample succession S1 to S4: (1) a broadening of the "cristobalite" peaks; (2) shifts of the peaks related to the tridymitic species, the positions of which approach those of the corresponding peaks for monoclinic tridymite; and (3) a gradual increase in the relative intensities of the "tridymite" peaks. The value of the dimensionless quantity

$$\eta = \frac{I(R2) + I(R3)}{I(R1) + I(R2) + I(R3) + I(R4)}$$

where I is the integrated intensity and $R1$, $R2$, $R3$, and $R4$ des-

Brought to you by | Florida Atlantic University
Authenticated
Download Date | 11/3/15 9:59 AM

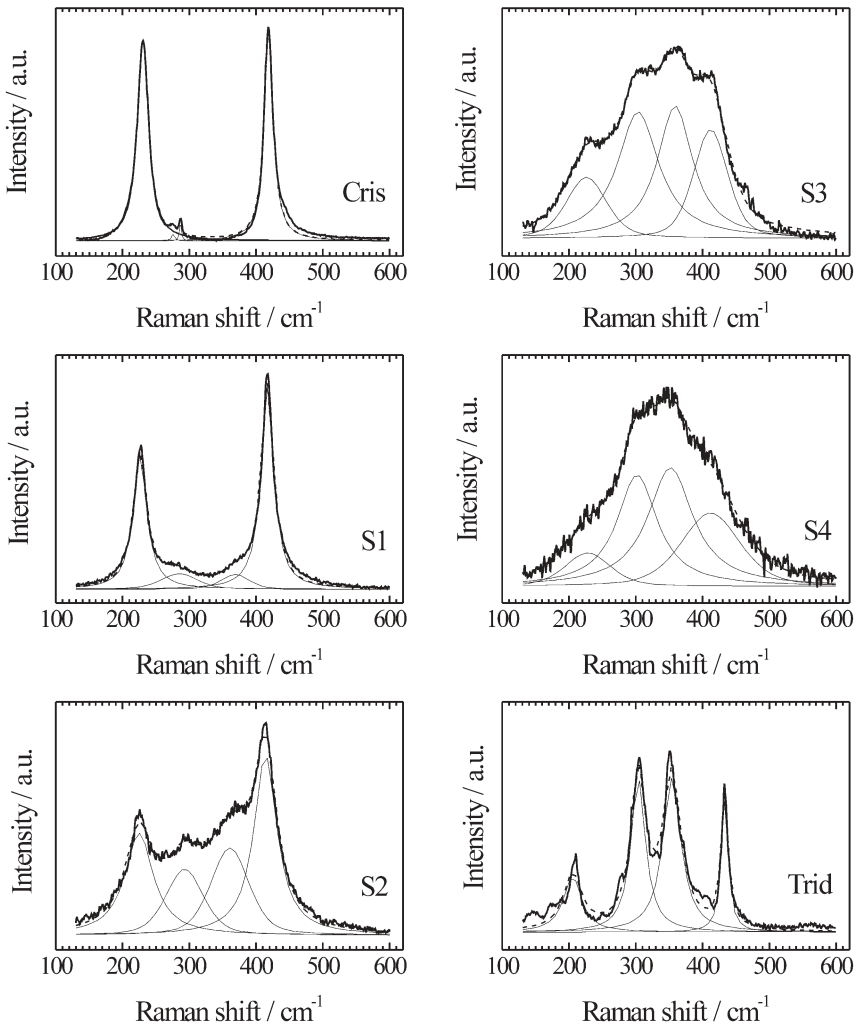

FIGURE 5. Non-linear curve fitting of Raman spectra of samples S1–S4 compared with the spectra of cristobalite and monoclinic tridymite.

ignate the Raman scattering near 225, 300, 350, and 415 cm^{-1}, respectively, can be used to estimate the tridymitic fraction in microcrystalline opal.

The trends in the Raman peak parameters are consistent with the increase in width of the major Bragg reflections and reveal the gradual change in the structural state from a predominantly cristobalite-like to a predominantly tridymite-like topology. For S3 and S4 the parameter η is larger than 0.5, i.e., the tridymite-like structural species dominate over the cristobalite-like species. The Raman peak widths offer additional information about the opal structure. A larger width is indicative of a greater variation in the atomic structural units that give rise to the corresponding peaks. By considering the parameter $\xi = \Gamma(R3)/\Gamma(R4)$, where Γ is the peak width, one can quantify the difference in the structural state of samples S3 and S4, which have nearly the same value of η. For S3, ξ is close to unity, which indicates the same degree of defectiveness in tridymitic and cristobalitic nano-regions. For S4, ξ is smaller than unity, revealing a higher degree of disorder in the cristobalite-like structural species than in the tridymite-like spatial regions; the large width of the peak near 412 cm^{-1} suggests a substantial structural variation in the cristobalite-like structural units. Thus, Raman spectroscopic data show that opals classified as opal-CT based on their XRD patterns may be of the opal-T type: its fundamental structural component can be regarded as a disordered tridymite-like matrix which incorporates atomic arrangements resembling to a certain extent the framework topology of cristobalite.

Furthermore, we analyzed the structure of opal samples from Neogene sediments and from different levels of the Palaeogene volcano-sedimentary complex in East Rhodopes (Fig. 6). For all of the samples the strongest diffraction maximum corresponds to a *d*-spacing of about 4.10 Å, with a less intense peak near 4.30 Å and a shoulder at about 3.90 Å. Thus, according to the accepted classifications, samples S5–S7 are opal-CT. The Raman spectra of samples S5–S8 are presented in Figure 6b. The opal samples (S5–S7) display an intense broad band centered in the range 330–360 cm^{-1}, which suggests the predominance of tridymite-type structural species. The bentonite sample S8 from the lower

Brought to you by | Florida Atlantic University
Authenticated
Download Date | 11/3/15 9:59 AM

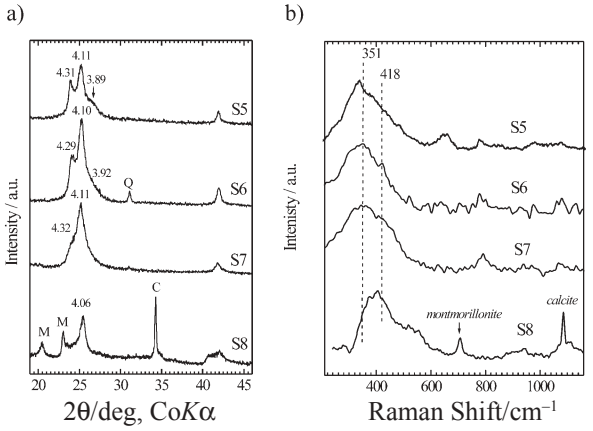

FIGURE 6. (**a**) XRD patterns and (**b**) Raman spectra of samples: S5 (Neogene), S6, S7 (upper levels of Ol_1), and S8 (lower levels of Ol_1); Q, M, and C in **a** denote the most intense Bragg reflections of quartz, montmorillonite, and calcite, respectively; the dotted lines in **b** trace the wavenumbers 351 and 418 cm^{-1}, which correspond to the position of the most intense Raman peak of α-tridymite and α-cristobalite, respectively.

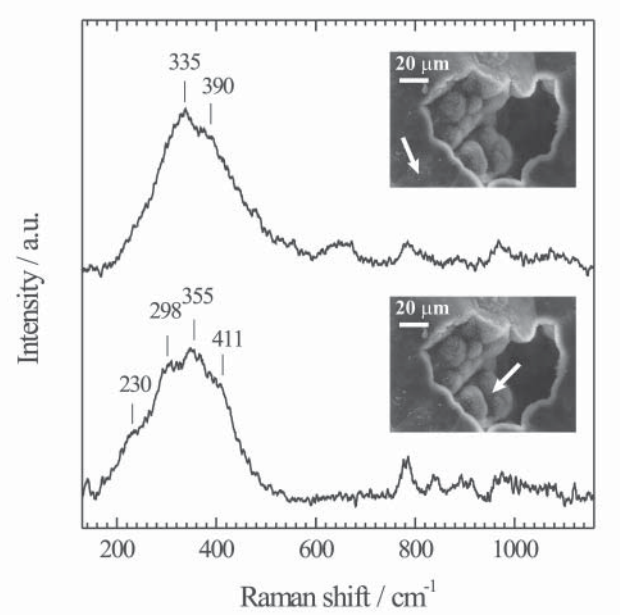

FIGURE 7. Raman spectra recorded from the main substance and lepispheres of S5; the arrows in the corresponding SEM images point to of the probed areas.

levels of Ol_1 of the Palaeogene volcano-sedimentary complex shows an intense Raman band shifted to higher wavenumbers and centered closer to the characteristic Raman peak of cristobalite. Unfortunately, clear conclusions about the structural state of the microcrystalline opal in S8 cannot be drawn only on the basis of the Raman data, since the contribution of montmorillonite in the range 300–500 cm^{-1} is considerable. However, the powder XRD pattern of the bentonite sample S8 displays a well-resolved Bragg reflection at about 4.06 Å, thus revealing an abundance of cristobalitic domains in the opal. Therefore, the opal component in the clay fraction is of the opal-C type. Samples S5–S7 should represent an earlier stage of diagenetic alteration of opal as compared with S8. Thus, our results are in accord with the phase formation sequence characteristic for the process of the maturation of silica (Iijima 1988).

Lepispheres have attracted great interest because of their occurrence in opals of different geneses. The complexity and the size of these aggregates make it difficult to determine their structure. They are composed of small crystal blades with a structure corresponding to opal-CT, although the crystallites are intergrown according to the tridymitic twin law (Flörke et al. 1976). Figure 7 shows the spectra collected from the main substance and from lepispheres of sample S5. The Raman spectrum of the lepispheres is similar to that of the main substance, but the primary band between 200 and 500 cm^{-1} is better structured, pointing to a higher degree of order. Lepispheres in more than a dozen cavities were examined and the corresponding spectra resembled the one shown in Figure 7. Thus, the Raman microspectroscopic data show that the structural state of lepispheres can be considered as a defect-rich tridymite-type matrix with nano-sized cristobalite-type structural entities.

In summary, the application of Raman spectroscopy is essential for the structural characterization of microcrystalline opals and for the estimation of the content of tridymite-like structural species, particularly on a scale finer than typically analyzed by XRD. Using this technique, we demonstrate for a series of opaline samples from the East Rhodopes volcanogenic-sedimentary complex that some samples have a prevalence of tridymitic atomic arrangements although their powder XRD patterns correspond to the opal-CT type according to the accepted classification. Opal specimens exhibiting the most intense poorly resolved Raman band centered near 330–360 cm^{-1} can be considered as opal-T, that is, the proportion of spatial regions with tridymite-type framework topology is higher than that of cristobalite-type framework topology.

The opal samples studied exhibit different structural states depending on their specific formation conditions and stratigraphic position in the Paleogene volcano-sedimentary complex in East Rhodopes: (1) the largest fraction of cristobalitic structural species was observed for opal from geodes; (2) opal deposited in upper geode bands (S3) exhibits a larger proportion of tridymitic domains than wall-banded opal (S1, S2); and (3) opals from bedded and lenticular opaline silicates deposited in marine conditions from hot Si-rich solutions (samples S4, S6–S8) and from opalized wood in Neogene sandstones (S5) exhibit a tridymite-type major structural component.

Raman micro-spectroscopy gives evidence that the principal structural component of lepispheres resembles the intermediate-range ordering of tridymite framework.

ACKNOWLEDGMENTS

We thank Bernd Güttler (PTB-Braunchweig) for enabling Raman micro-spectroscopic measurements in his laboratory, Jochen Schlüter (Mineralogical Museum, University of Hamburg) for providing the reference cristobalite and tridymite samples, and David Bish for the critical reading of the manuscript. Financial support by the National Science Fund, Bulgarian Ministry of Science (F-1212, NT 1-02) is gratefully acknowledged. We express our gratitude to the reviewers and the associate editor for their valuable comments and constructive criticism, which helped us to improve the original manuscript.

Brought to you by | Florida Atlantic University
Authenticated
Download Date | 11/3/15 9:59 AM

REFERENCES CITED

Adams, S.J., Hawkes, G.E., and Curzon, E.H. (1991) A solid state ^{29}Si nuclear magnetic resonance study of opal and other hydrous silicas. American Mineralogist, 76, 1863–1871.

Akizuki, M. and Shimada, I. (1979) Texture and minerals in opal from Hosaka, Fukushima Prefecture, Japan. Journal of the Japanese Association of Mineralogy, Petrology and Economical Geology, 74, 274–279 (in Japanese).

Barrio, R.A., Galeener, F.L., Martinez, E., and Elliott, R.J. (1993) Regular ring dynamics in AX2 tetrahedral glasses. Physical Review B, 48, 15672–15689.

De Jong, B.H.W.S., van Hock, J., Veeman, W.S., and Manson, D.V. (1987) X-ray diffraction and ^{29}Si magic-angle-spinning NMR of opals: Incoherent long- and short-range order in opal-CT. American Mineralogist, 72, 1195–1203.

Dutta, P.K., Rao, K.M., and Park, J.Y. (1991) Correlation of Raman spectra of zeolites with framework architecture. Journal of Physical Chemistry, 95, 6654–6657.

Elzea, J.M. and Rice, S.B. (1996) TEM and X-ray diffraction evidence for cristobalite and tridymite stacking sequences in opal. Clays and Clay Minerals, 44, 492–500.

Elzea, J.M., Odom, I.E., and Miles, W.J. (1994) Distinguishing well ordered opal-CT and opal-C from high-temperature cristobalite by X-ray diffraction. Analytica Chimica Acta, 286, 107–116.

Etchepare, J., Merian, M., and Kaplan, P. (1978) Vibrational normal modes of SiO_2. II. Cristobalite and tridymite. Journal of Chemical Physics, 68, 1531–1537.

Flörke, O.W., Hollmann, R., Von Rad, U., and Roesch, H. (1976) Intergrowth and twinning in opal-CT lepispheres. Contributions to Mineralogy and Petrology, 58, 235–242.

Flörke, O.W., Graetsch, H., Martn, B., Roller, K., and Wirth, R. (1991) Nomenclature of micro- and non-crystalline silica minerals, based on structure and microstructure. Neues Jahrbuch für Mineralogie-Abhandlungen, 163, 19–42.

Fritsch, E., Gaillou, E., Ostroumov, M., Rondeau, B., Devouard, B., and Barreau, A. (2004) Relationship between nanostructure and optical absorption in fibrous pink opals from Mexico and Peru. European Journal of Mineralogy, 16, 743–752.

Gage, D.R. and Farwell, S.O. (1981) Laser Raman spectrometry for the determination of crystalline silica polymorphs in volcanic ash. Analytical Chemistry, 53, 2123–2127.

Graetsch, H. (1994) Structural characteristics of opaline and microcrystalline silica minerals. In P.J. Heaney, C.T. Prewitt, G.V. Gibbs, Eds., Silica, 29, p. 209–232 and references therein. Reviews in Mineralogy, Mineralogical Society of America, Chantilly, Virginia.

Graetsch, H., Gies, H., and Topalović, I. (1994) NMR, XRD and IR srudy on microcrystalline opals. Physics and Chemistry of Minerals, 21, 166–175.

Guthrie, G.D. Jr., Bish, D.L., and Reynolds, R.S. Jr. (1995) Modeling the X-ray diffraction pattern of opal-CT. American Mineralogist, 80, 869–872.

Hirose, T., Kihara, K., Okuno, M., Fujinami, S., and Shinoda, K. (2005) X-ray, DTA and Raman studies of monoclinic tridymite and its higher temperature orthorhombic modification with varying temperature. Journal of Mineralogical and Petrological Sciences, 100, 55–69.

Iijima, A. (1988) Diagenetic transformations of minerals as exemplified by zeolites and silica minerals. Part II. Silica diagenesis. In G.V. Chilingarian and K.H. Wolf, Eds., Diagenesis II, 43, p. 189–209. Developments in Sedimentology, Elsevier, Amsterdam.

Jones, J.B. and Segnit, I.R. (1971) The nature of opal. I. Nomenclature and constituent phases. Journal of the Geological Society of Australia, 18, 57–68.

Kihara, K., Hirose, T., and Shinoda, K. (2005) Raman spectra, normal modes and disorder in monoclinic tridymite and its higher temperature orthorhombic modification. Journal of Mineralogical and Petrological Sciences, 100, 91–103.

Kingma, K.J. and Hemley, R. J. (1994) Raman spectroscopic study of microcrystalline silica. American Mineralogist, 79, 269–273.

Krumm, S. (1994) "WINFIT 1.0—A computer program for X-ray diffraction line profile analysis," XIII Conference on Clay Mineralogy and Petrology. Acta Universitatis Carolinae Geologica, 38, 253–261.

Lazzeri, M. and Mauri, F. (2003) First-principle calculation of vibrational Raman spectra in large system: signature of small rings in crystalline SiO_2. Physical Review Letters, 90, 036401-1–036401-4.

Mihailova, B. and Konstantinov, L. (1997) Dependence of vibrational spectra of rings of SiO_4 tetrahedra on their structural parameters. Solid State Communications, 101, 163–166.

Nagase, T. and Akizuki, M. (1997) Texture and structure of opal-CT and opal-C in volcanic rocks. Canadian Mineralogist, 35, 947–958.

Ostrooumov, M., Fritsch, E., Lasnier, B., and Lefrant, S. (1999) Spectres Raman des opals: aspect diagnostique et aide a la classification. European Journal of Mineralogy, 11, 899–908.

Rice, S.B., Freund, H., Clouse, J.A., Fleissner, T.G., and Isaacs, C.M. (1995) Application of Fourier transform infrared spectroscopy to silica diagenesis: the opal-A to opal-CT transformation, A. Sedimentary Processes. Journal of Sedimentary Research, A65, 639–647.

Rodgers, K.A. and Hampton, W.A. (2003) Laser Raman identification of silica phases comprising microtextural components of sinters. Mineralogical Magazine, 67, 1–13.

Sharma, S.K., Mammone, J.F., and Nicol, M.F. (1981) Raman investigation of ring configurations in vitreous silica. Nature, 292, 140–142.

Smallwood, A.G., Thomas, P.S., and Ray, A.S. (1997) Characterisation of sedimentary opals by Fourier transform Raman spectroscopy. Spectrochimica Acta Part A, 53, 2341–2345.

Smith, D.K. (1998) Opal, cristobalite, and tridymite: Noncrystallinity versus crystallinity, nomenclature of silica minerals and bibliography. Powder Diffraction, 13, 2–19.

Sykes, D. and Kubicki, J.D. (1996) Four-membered rings in silica and aluminosilicate glasses. American Mineralogist, 81, 265– 273.

Wilson, M.J., Russell, J.D., and Tate, J.M. (1974) A new interpretation of the structure of disordered α-cristobalite. Contributions to Mineralogy and Petrology, 47, 1–6.

MANUSCRIPT RECEIVED OCTOBER 17, 2006
MANUSCRIPT ACCEPTED MAY 9, 2007
MANUSCRIPT HANDLED BY BRIGITTE WOPENKA

Brought to you by | Florida Atlantic University
Authenticated
Download Date | 11/3/15 9:59 AM